# Structure and nonlinear optical properties of novel transparent glass-ceramics based on Co2+:ZnO nanocrystals

**Article** *in* Laser Physics Letters · May 2016

Impact Factor: 2.46 · DOI: 10.1088/1612-2011/13/5/055803



**12 authors**, including:

Pavel Loiko

KTH Royal Institute of Technology

**92** PUBLICATIONS **372** CITATIONS

SEE PROFILE

Olga Dymshits

Vavilov State Optical Institute

**95** PUBLICATIONS **574** CITATIONS

SEE PROFILE

Vladimir Vitkin

ITMO University

**10** PUBLICATIONS **2** CITATIONS

SEE PROFILE

K.V. Yumashev

Belarusian National Technical University

**291** PUBLICATIONS **2,511** CITATIONS

SEE PROFILE

IOP Publishing | Astro Ltd Laser Physics Letters
Laser Phys. Lett. 13 (2016) 055803 (7pp) doi:10.1088/1612-2011/13/5/055803

# Structure and nonlinear optical properties of novel transparent glass-ceramics based on $Co^{2+}$:ZnO nanocrystals

**P A Loiko[1], O S Dymshits[2], V V Vitkin[3], N A Skoptsov[1], A A Zhilin[2], D V Shemchuk[2], M Ya Tsenter[2], K V Bogdanov[3], A M Malyarevich[1], I V Glazunov[1], X Mateos[4] and K V Yumashev[1]**

[1] Center for Optical Materials and Technologies, Belarusian National Technical University, 65/17 Nezavisimosti Ave., Minsk 220013, Belarus
[2] NITIOM S.I. Vavilov State Optical Institute, #36, Babushkina Str., St Petersburg 192171, Russia
[3] ITMO University, 49 Kronverkskiy pr., Saint-Petersburg 197101, Russia
[4] Física i Cristal·lografia de Materials i Nanomaterials (FiCMA-FiCNA), Universitat Rovira i Virgili (URV), Campus Sescelades, c/ Marcel·lí Domingo, s/n., Tarragona E-43007, Spain

E-mail: kinetic@tut.by

Received 27 August 2015, revised 22 March 2016
Accepted for publication 23 March 2016
Published 8 April 2016

**Abstract**

Transparent glass-ceramics (GCs) based on $Co^{2+}$:ZnO nanocrystals (mean diameter, 11 nm) are synthesized on the basis of cobalt-doped glasses of the $K_2O$–ZnO–$Al_2O_3$–$SiO_2$ system. For these GCs, the absorption band related to the $^4A_2(^4F) \rightarrow {}^4T_1(^4F)$ transition of $Co^{2+}$ ions in tetrahedral sites spans until ~1.73 $\mu$m. Saturation of the absorption is demonstrated at 1.54 $\mu$m, with a saturation fluence $F_s = 0.8 \pm 0.1$ Jcm$^{-2}$ ($\sigma_{GSA} = 1.7 \pm 0.2 \times 10^{-19}$ cm$^2$) and a recovery time of 890 $\pm$ 10 ns. Passive Q-switching of an Er,Yb:glass laser is realized with the synthesized GCs. This laser generated 0.37 mJ/100 ns pulses at 1.54 $\mu$m. The developed GCs are promising as saturable absorbers for 1.6–1.7 $\mu$m crystalline erbium lasers.

Keywords: glass-ceramics, cobalt, zinc oxide, erbium laser, Q-switching

(Some figures may appear in colour only in the online journal)

## 1. Introduction

Erbium ($Er^{3+}$) ions are attractive due to their eye-safe emission around 1.5 $\mu$m related to the $^4I_{13/2} \rightarrow {}^4I_{15/2}$ transition. Pulsed erbium lasers are of practical importance for range-finding, environmental sensing, aerial navigation, telecom applications and laser surgery.

There are two main schemes for the excitation of $Er^{3+}$ ions. The first one is codoping the host with the ($Er^{3+}$,$Yb^{3+}$) couple. $Yb^{3+}$ ions can be efficiently pumped at ~0.98 $\mu$m by commercial InGaAs laser diodes; the subsequent excitation of $Er^{3+}$ ions occurs due to the energy-transfer (ET), $^2F_{5/2}$ ($Yb^{3+}$) $\rightarrow {}^4I_{11/2}$($Er^{3+}$). However, this scheme suffers from a strong up-conversion related to the ET process (that generates a lot of unwanted heat and limits the laser efficiency). It also requires careful optimization of dopant concentrations, thermal and thermo-optical properties and vibrational frequencies of the host. State-of-the-art materials for ($Er^{3+}$,$Yb^{3+}$) codoping are phosphate glasses providing very high efficiencies of the ET but possessing very poor thermal properties [1]. Thus, several crystalline materials were proposed as an alternative for the glass in terms of thermo-mechanical properties, however, only a few of them, basically borates such as $REAl_3(BO_3)_4$ where RE = Y, Gd or Lu [2–4] can compete with phosphate glasses in terms of ET efficiency. In addition, they provide low thermo-optic aberrations [5].

Phosphate glass [6, 7] and crystalline borate [8] lasers can be efficiently Q-switched by Co:$MgAl_2O_4$ spinel single crystals using the saturable absorption related to the $^4A_2(^4F) \rightarrow {}^4T_1(^4F)$ transition of tetrahedrally coordinated

 

$Co^{2+}$ ions. Indeed, the emission wavelengths of these lasers (1.54 … 1.60 $\mu$m) perfectly match the absorption band of Co:$MgAl_2O_4$ single crystals.

The second scheme for the excitation of Er lasers is the so-called resonant (in-band) pumping. Such a direct excitation to the upper laser level of $Er^{3+}$, $^4I_{13/2}$, can be achieved by Er fiber lasers or InGaAsP/InP laser diodes emitting at ~1.5 $\mu$m. Several high-energy crystalline in-band-pumped Er lasers were recently realized emitting typically at wavelengths longer than 1.6 $\mu$m [9–11]. In particular, the Er:YAG crystal provides a laser emission at 1645 nm [11], where the use of the Co:$MgAl_2O_4$ single crystal is no longer efficient due to an increased saturation fluence. Thus, the search for novel saturable absorbers (SAs) operating in the 1.6–1.7 $\mu$m spectral range is of high importance for efficient Q-switching of Er crystalline lasers.

Transparent $Co^{2+}$-doped spinel-based nanophase glass-ceramics (GCs) were recognized as a good alternative to Co:$MgAl_2O_4$ single crystals. They typically contain nano-sized crystals of Mg-spinel $MgAl_2O_4$ or gahnite $ZnAl_2O_4$ [12, 13] or ɣ-$Ga_2O_3$ [14] with $Co^{2+}$ ions incorporated in sites with tetrahedral symmetry. As compared with single crystals, GCs offer an easier synthesis technique based on the standard glass melt-quenching method with a subsequent heat-treatment; GCs provide relatively low scattering losses ($\alpha_{loss} < 0.1\,cm^{-1}$ at ~1.6 $\mu$m) [12]. Synthesis of novel GCs wherein the local environment of $Co^{2+}$ ions could provide a lower ligand field than in spinel crystals, which would result in a red-shift of $Co^{2+}$ spectral bands, can solve the above-mentioned problem of the lack of long-wavelength SAs.

In the present letter, we report on the synthesis, structure and nonlinear optical properties of novel transparent GCs containing nanosized $Co^{2+}$:ZnO crystals suitable for passive Q-switching of crystalline erbium lasers emitting at 1.6–1.7 $\mu$m.

## 2. Synthesis of glass-ceramics

The glass with the composition (wt%) 15$K_2O$–30ZnO–16$Al_2O_3$–39$SiO_2$ [15, 16] was doped with 0.05 or 0.1 wt% CoO. The starting materials for the glass preparation included reagent grade $K_2CO_3$, ZnO, $Al_2O_3$ and $SiO_2$. The appropriate components were carefully mixed and glasses 200 g in weight were melted in platinum crucibles in a laboratory electric furnace at 1590 °C for 3 h with stirring, cast onto a cold metal plate and annealed at 550 °C in an electric furnace. The temperature of secondary heat-treatments was ranged from 650 to 750 °C, the heating rate was 5 °C per min; the heat-treatment duration was 2–24 h. The initial glasses were transparent and violet–blue colored, after the heat-treatment, they remained transparent while their color changed to blue–green.

## 3. Results and discussion

### 3.1. Structural study

Phase assemblages of initial and heat-treated glasses were identified using x-ray powder diffraction technique (using a Shimadzu 6000 diffractometer, Cu K$\alpha$ radiation with a Ni filter). The detected x-ray diffraction (XRD) patterns of the initial glass and GCs are shown in figure 1. The mean crystal sizes were estimated from the broadening of the x-ray peaks according to [17]:

$$D = K\lambda/\Delta(2\theta)\cos\theta, \quad (1)$$

where $\lambda$ is the x-ray radiation wavelength, $\theta$ is the diffraction angle, $\Delta(2\theta)$ is the width of the peak at half of its maximum, and $K$ is a constant that was assumed to be 1 [17]. The error of the crystal size estimation was ~5% for the crystal sizes of 2–15 nm.

The initial glasses were x-ray amorphous, figure 1. The heat-treatments in the temperature range of 680–700 °C resulted in crystallization of ZnO nanocrystals with a hexagonal wurtzite structure, with all zinc and oxygen ions with tetrahedral coordination [15]. Their mean sizes were about 11 nm.

Phase transformations in the initial glasses as a result of heat-treatments were also studied by Raman spectroscopy,

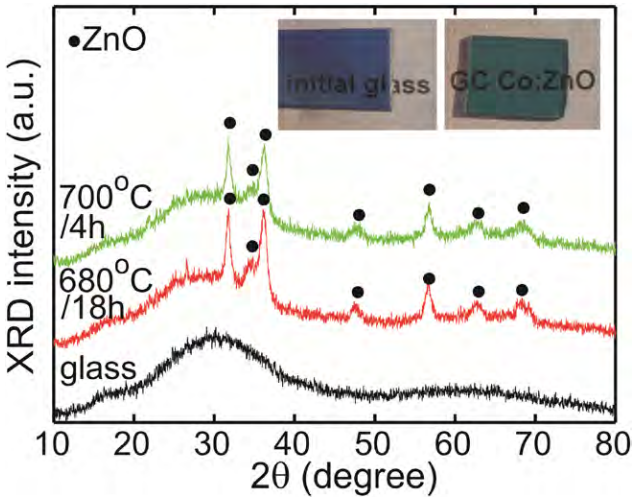


**Figure 1.** XRD patterns of initial and heat-treated glasses doped with 0.05 wt% CoO, *inset*: images of the polished samples lying on the paper with the typed text 'initial glass' and 'GC Co:ZnO'.

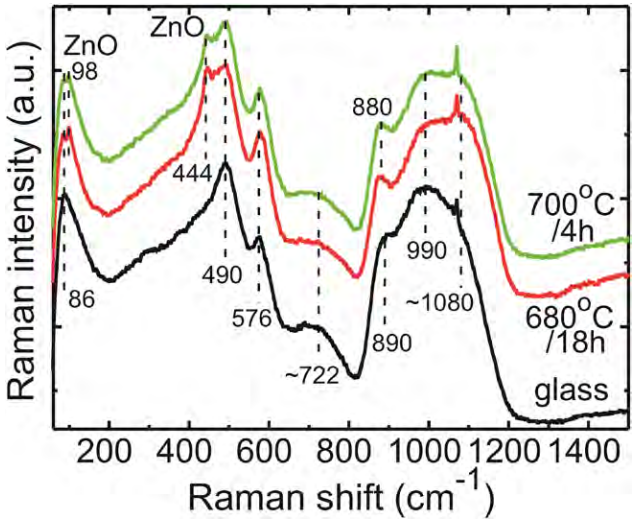


**Figure 2.** Raman spectra of initial and heat-treated glasses doped with 0.05 wt% CoO. The excitation wavelength is 488 nm.

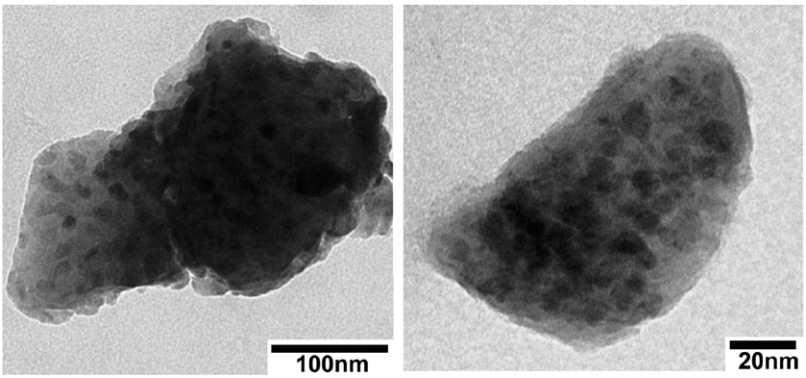


**Figure 3.** TEM images of the GC doped with 0.1 wt% CoO and prepared by heat-treatment at 700 °C for 24 h.

figure 2. The Raman spectra were recorded in backscattering geometry by using an 'InVia' (Renishaw, England) Micro-Raman spectrometer equipped with the multichannel detector cooled down to −70 °C. The $Ar^+$ laser line of 488 nm was employed as an excitation source. A Leica 50 × (NA = 0.75) objective was used for illuminating the sample and the scattered light was collected by the same objective. An edge filter was placed before the spectrograph entrance slit. A spatial resolution of 2 $cm^{-1}$ was obtained. The acquisition time was 60 s.

The Raman spectrum of the initial glass consists of a high-frequency envelope with maxima at ~890, 990 and 1080 $cm^{-1}$, the main band with peaks at 490, 576 and 722 $cm^{-1}$, and the boson peak at ~86 $cm^{-1}$. A similar Raman spectrum with slightly different frequencies of peaks was obtained by Du *et al* [18] for a glass of the same system with a similar composition $15K_2O$–$25ZnO$–$15Al_2O_3$–$45SiO_2$ (in mol%). After the heat-treatment of the initial glass, the shape of the high-frequency envelope in its spectrum changes due to the intensity increase of the band at 1080 $cm^{-1}$. Two new sharp peaks appear at 98 and 444 $cm^{-1}$.They can be assigned to the $E_2$ (low) and $E_2$ (high) modes of wurtzite ZnO crystals, respectively [18–20]. The $E_2$ (low) mode is related to the vibration of the heavy Zn sublattice and the $E_2$ (high) mode involves only oxygen atoms [19]. The intensity enhancement of the band at 1080 $cm^{-1}$ of the high-frequency envelope can be explained by the increased connectivity of the aluminosilicate network caused by the ZnO crystallization. The initial glass composition in mol% was $12K_2O$–$28ZnO$–$12Al_2O_3$–$48SiO_2$. In the assumption that all the ZnO participates in the crystallization, the residual glass composition can be expressed as $16.7K_2O$–$16.7Al_2O_3$–$66.6SiO_2$, i.e. $K_2O{\cdot}Al_2O_3{\cdot}4SiO_2$, or $KAlSi_2O_6$, which matches the composition of mineral leucite. We are not aware of the existence of the spectrum of a glass with leucite composition in the literature, however, the spectrum of amorphous leucite obtained at high pressure is known [21] and its high-frequency envelope is consistent with those of the glass-ceramics obtained in this work. The Raman spectra of the $SiO_2$–$KAlSi_3O_8$ glass series [22] also demonstrate similar features. It is unlikely that the residual glass having potassium cations in sufficient quantity to charge balance the four-fold coordinated $Al^{3+}$ contains a significant number of non-bridging oxygen atoms. On this basis, it is inferred that high-frequency features in the glass-ceramic spectrum result primarily from the antisymmetric-stretching modes of O atoms and network-forming cations in the 3D aluminosilicate framework [23].

The structure of the glass-ceramics was also studied by transmission electron microscopy (TEM). For TEM studies, finely powdered samples were dispersed in ethanol. The microscope used was a JEOL TEM-1011 (100 kV acceleration voltage, 0.4 nm point resolution). The sample obtained by heat-treatment at 700 °C for 24 h and containing ZnO nanocrystals, as determined by the XRD analysis, was investigated. The TEM images (figure 3) reveal a near-uniform distribution of inhomogeneous dark regions. We refer these regions to the nanosized ZnO crystals located in the residual glassy phase. The average size of nanocrystals $D_{TEM}$ is 11.2 ± 0.4 nm that agrees well with $D_{XRD}$ (~11 nm); and their shape is nearly spherical.

### 3.2. Optical absorption

For the optical absorption measurements, we used Varian CARY-5000 spectrophotometer. The samples were plates polished down to ~0.4 mm.

The absorption spectra of the initial glass and glass-ceramics are shown in figure 4. The spectrum of the initial glass is typical for absorption of $Co^{2+}$ ions in aluminosilicate glasses [24, 25]. The spectrum contains two broad structured absorption bands in the 470–720 nm (21 000–14 000 $cm^{-1}$) and 1100–1700 nm (9000–5800 $cm^{-1}$) ranges with local peaks at 525/590/640 nm and 1235/1455/1660 nm. This type of the spectrum is characteristic of $Co^{2+}$ ions in a distorted tetrahedral coordination in silicate glasses [26, 27]. However, the relatively low intensity of the absorption bands suggests the contribution of $Co^{2+}$ ions in octahedral and possibly in 5-fold coordinated sites [24, 28, 29]. Their absorption at ~525 nm coincides with one of the peaks related to the absorption of $Co^{2+}$ ions in a distorted tetrahedral coordination [24, 28, 29].

Crystallization of ZnO is accompanied by a change in the absorption spectrum. The UV absorption edge of the initial glass shifts to the visible due to the crystallization of ZnO; its position depends on the heat-treatment applied. The intensity of both absorption bands continuously increases and their shape is changed. In the visible part of the spectrum, there is a gradual reduction of absorption at ~525 nm, an appearance of a shoulder at ~565 nm, a shift of the absorption bands at 590 and 640 nm to 607 and 643 nm, respectively, and an increase

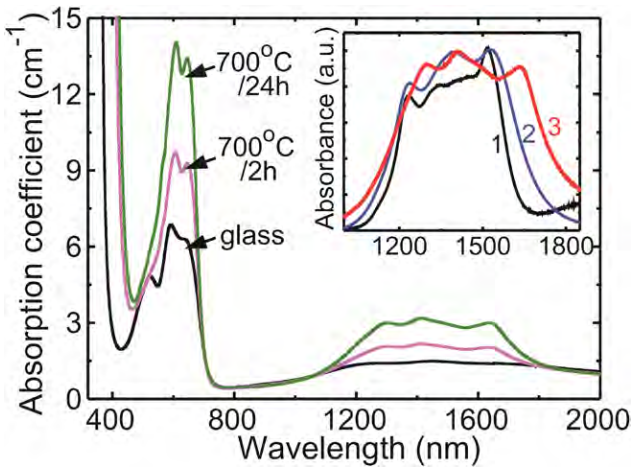


**Figure 4.** Absorption spectra of the initial glass and GC doped with 0.1 wt% CoO, *inset*: absorption band related to the $^4A_2(^4F) \rightarrow {}^4T_1(^4F)$ transition of $Co^{2+}$ ions in tetrahedral sites in (1) Co:$MgAl_2O_4$ single-crystal and GC containing (2) Co:$MgAl_2O_4$ and (3) Co:ZnO nanocrystals.

of their intensity. The broad band in the 1.2–1.7 $\mu$m range becomes narrower; the peaks become more distinct than in the spectrum of the initial glass. This broad band is composed of four separate peaks located at ~1.29, 1.42, 1.49 and 1.64 $\mu$m.

The absorption bands observed for GCs coincide well with the ones for $Co^{2+}$:ZnO [30, 31] and they can be ascribed to the d–d transitions of $Co^{2+}$ ions with $3d^7$ high-spin configuration in a tetrahedral ligand field formed by neighboring oxygen ions in ZnO nanocrystals. Three absorption peaks in the visible range are assigned as $^4A_2(F) \rightarrow {}^2E(G)$, $^4A_2(F) \rightarrow {}^4T_1(P)$, and $^4A_2(F) \rightarrow {}^2A_1(G)$ transitions. The absorption band in the infrared is associated with the electronic transitions from the $^4A_2(F)$ ground-state to the $^4T_1(F)$ excited multiplet. This is actually the band intended to be used for Q-switching of erbium lasers. The above-mentioned spectral changes indicate an appearance of undistorted tetrahedrally coordinated $Co^{2+}$ ions in ZnO nanocrystals at the expense of the $Co^{2+}$ ions located in the initial glass.They are clearly connected with the ZnO crystallization and entering the $Co^{2+}$ ions in its structure in the positions of $Zn^{2+}$ ions [15, 16, 30]. The increase of fraction of ZnO is accompanied by the increase of absorption of tetrahedrally coordinated $Co^{2+}$ ions. However, a careful comparison of the absorption spectra of the Co:ZnO based GCs and $Zn_{1-x}Co_xO$ powders [31] revealed that there is still an inflection at ~525 nm in the spectrum of the GCs and the intensity of the band at ~565 nm is lower that in the spectrum of the $Zn_{1-x}Co_xO$ powders. These facts led us to the conclusion that after the proposed heat-treatments at 680–700 °C, some portion of $Co^{2+}$ ions still remains in the residual glass phase.

In the inset of figure 4, we present a comparison of the absorption related to the $^4A_2(^4F) \rightarrow {}^4T_1(^4F)$ transition of $Co^{2+}$ ions in the GCs with Co:ZnO nanocrystals prepared by the heat-treatment at 700 °C, GCs containing Co:$MgAl_2O_4$ spinel nanocrystals and Co:$MgAl_2O_4$ single crystals. Then, we determined the long-wavelength edge $\lambda_{th}$ of this absorption band (corresponding to the half intensity of the peak absorption). For the GCs based on Co:ZnO nanocrystals, $\lambda_{th}$ =1.73 $\mu$m and it is only 1.58 $\mu$m for Co:$MgAl_2O_4$ single crystals and 1.63 $\mu$m for Co: $MgAl_2O_4$ based GCs. Thus, the proposed GCs are promising for passive Q-switching of erbium lasers emitting in the 1.6–1.7 $\mu$m spectral range.

### 3.3. Absorption saturation

For the absorption saturation experiment, the GC sample doped with 0.1 wt% CoO and containing $Co^{2+}$:ZnO nanocrystals was prepared at 700 °C for 24 h. It was 3.9 mm thick ($T_0$ = 42% at 1.54 $\mu$m; $\alpha_0$ =2.3 cm$^{-1}$).The sample was polished to laser quality and it was remained uncoated.

Absorption saturation was performed with the *Z*-scan technique. The excitation beam was generated by a flashlamp-pumped $Er^{3+}$,$Yb^{3+}$:glass laser passively Q-switched by a $Co^{2+}$: $MgAl_2O_4$ single crystal SA (pulse energy: ~2 mJ, pulse duration: 70 ns, $TEM_{00}$ output). The output of this laser was focused by a spherical lens ($f$ =35 mm) to a ~80 $\mu$m spot. The studied sample was translated along the beam in the longitudinal direction thus providing a variation of the incident fluence in the range of 0.4–12.0 J cm$^{-2}$.

The radius of the laser beam $w$ with respect to the axial coordinate ($z$) was measured with a CCD-camera. The incident pulse energy $E_{inc}$ was measured with an Ophir PE-10C energy meter with a precision of 0.1 mJ. The incident fluence on the sample was then calculated as $F_{inc}(z) = 2E_{inc}/[\pi w(z)^2]$ (the factor 2 emerges from the consideration of Gaussian spatial profile of the pump laser beam). After insertion of the sample, the pulse energy of the transmitted pump beam $E_{trans}(z)$ was measured. The internal power-dependent transmission of the studied sample was then determined as $T(z) = XY[E_{trans}(z)/E_{inc}]$ where $X$ is the correction factor due to the Fresnel losses and $Y$ is the calibration constant. To calibrate the set-up, we used a polished plate from an undoped silicate glass showing no absorption saturation. Then, taking into account the dependence $F_{inc}(z)$, the experimental curve $T(F_{inc})$ was achieved.

The experimental data on $T(F_{inc})$ were modeled with a slow SA model because the characteristic recovery time for $Co^{2+}$ ions is typically few hundreds of ns that is much shorter than the duration of the excitation pulse (in our case, ~70 ns). As the thickness of the studied sample was relatively long ($t$ ~ 3 mm), it cannot be considered as a thin SA. Thus, the following formula was used [12, 13]:

$$\frac{dF}{dz} = -\alpha_0 F_S\left[(1-\gamma)(1-e^{-F/F_S}) + \gamma\frac{F}{F_S}\right]. \qquad (2)$$

Here, $z$ denotes the axial coordinate inside the SA, $F_S = h\nu/\sigma_{GSA}$ is the saturation fluence of the studied material; $\gamma$ is the saturation contrast that is equal to $\sigma_{ESA}/\sigma_{GSA}$; $h$ is the Planck constant, $\nu = c/\lambda$ is the light frequency, $c$ is the speed of light; $\sigma_{ESA}$ and $\sigma_{GSA}$ are the cross-sections for the excited- and ground-state absorption (ESA and GSA) for the $Co^{2+}$ ions, respectively. In equation (2), $F_S$ and $\gamma$ are free parameters that were varied. For each incident fluence $F_{inc}$, equation (2) was solved for $z = 0...t$ and the theoretical transmitted energy

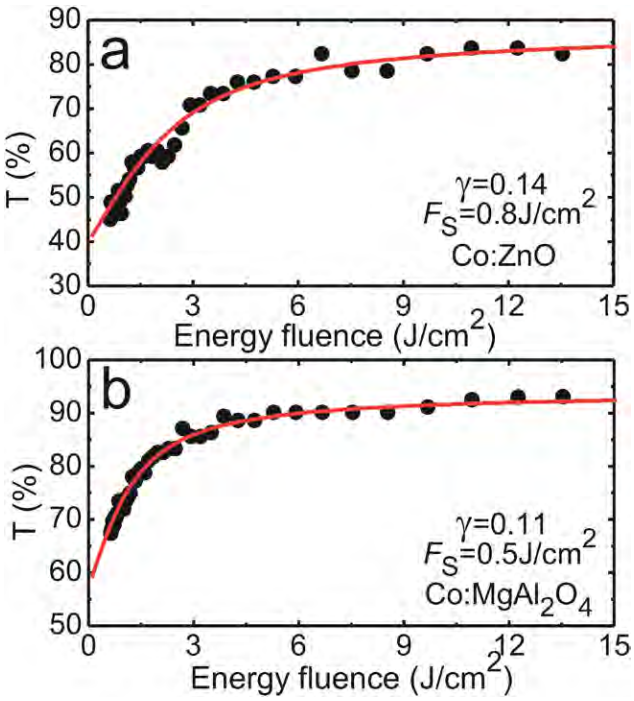


**Figure 5.** Absorption saturation curves for (a) Co:ZnO-based GC doped with 0.1 wt% CoO prepared at 700 °C for 24 h and (b) Co:$MgAl_2O_4$ single crystal.

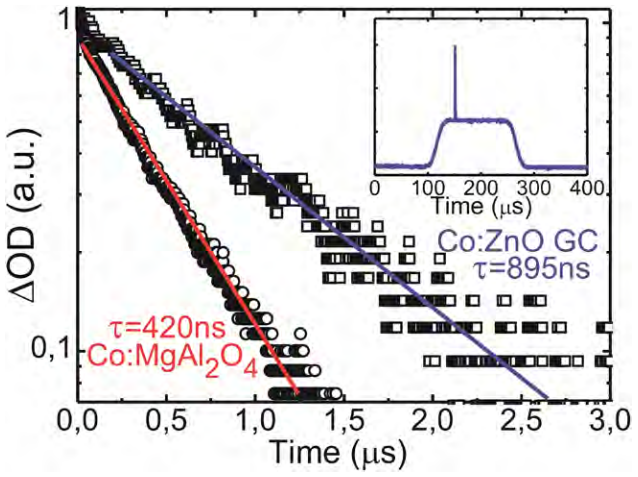


**Figure 6.** Semi-logarithmic plot of the differential optical density ΔOD as a function of time for GC with Co:ZnO nanocrystals and Co:$MgAl_2O_4$ single crystal, *symbols* represent the experimental data, *lines* are their modeling with a monoexponential law for the extraction of the recovery time ($\tau$), *inset* shows the typical as-measured oscilloscope trace.

fluence $F'_{trans}$ was found. Then, the theoretical transmission of the SA $T'(F_{inc}) = F'_{trans}/F_{inc}$ was determined. Finally, the experimental curve $T(F_{inc})$ was fitted with the theoretical one, $T'(F_{inc})$, yielding $F_S$ and $\gamma$ parameters.

For the GC containing Co:ZnO nanocrystals, the best fitting parameters for the absorption saturation curve are $F_S = 0.8 \pm 0.1$ Jcm$^{-2}$ and $\gamma = 0.14 \pm 0.02$, figure 5(a), which are close to the same parameters determined for the Co:$MgAl_2O_4$ single crystal, $F_S = 0.5 \pm 0.1$ Jcm$^{-2}$ and $\gamma = 0.11 \pm 0.02$, see figure 5(b). The ground-state absorption cross-section $\sigma_{GSA}$ for the $Co^{2+}$ ions in the ZnO nanocrystals is ~$1.7 \pm 0.2 \times 10^{-19}$ cm$^2$ at 1.54 $\mu$m; and the value for the excited-state absorption cross-section is $\sigma_{ESA} = 0.24 \pm 0.05 \times 10^{-19}$ cm$^2$. The laser damage threshold for the glass-ceramics with Co:ZnO nanocrystals was determined to be as high as ~$14 \pm 2$ Jcm$^{-2}$.

### 3.4. Recovery time

To measure the characteristic recovery time of the initial absorption of the $Co^{2+}$ ions ($\tau$), we employed the pump-probe method. The studied sample was excited by the output of a flashlamp-pumped $Er^{3+}$,$Yb^{3+}$:glass laser passively Q-switched by a $Co^{2+}$:$MgAl_2O_4$ single crystal SA (pulse energy: 4 mJ, pulse duration: ~70 ns, multimode output). The pump beam was focused onto the sample to a spot of ~500 $\mu$m in diameter providing a maximum pump fluence of ~10 Jcm$^{-2}$ that corresponded to a near-complete bleaching of the sample but was slightly below the laser damage threshold. The pump wavelength was ~1.54 $\mu$m that corresponded to the $^4A_2(^4F) \rightarrow {}^4T_1(^4F)$ transition of the $Co^{2+}$ ions in tetrahedral sites. As a probe beam, we used the output of a continuous-wave He–Ne laser (632.8 nm) that was modulated by a mechanical chopper (frequency: 550 Hz, pulse duration: 160 $\mu$s). The probe wavelength corresponded to the $^4A_2(^4F) \rightarrow {}^4T_1(^4P)$ transition for tetrahedrally coordinated $Co^{2+}$ ions. Thus, we were able to monitor the recovery of the initial population of the $^4A_2(^4F)$ ground-state that determines the $\tau$ value. In addition, the large spectral separation of the pump and probe beams simplified their detection. To detect the probe beam, a fast Hamamatsu C5460 photodetector (response time, <40 ns) and a 500 MHz Tektronix TDS-3052B digital oscilloscope were used.

As a result of the ground-state depletion of the $Co^{2+}$ ions by the pump pulse, the transmission of the probe beam temporarily increased. The differential absorption was then determined. It reads $\Delta OD(t) = \ln[T(t)/T_0]$, where $T_0$ is the initial (non-saturated) transmission of the sample, and $T(t)$ is its transmission at a time $t$ after the end of the pump pulse. The recovery time $\tau$ was then deduced by fitting the curve to an exponential decay in the form:

$$\Delta OD(t) = \Delta OD_{max} \exp(-t/\tau). \quad (3)$$

For the recovery time measurements, we used the same sample as for the absorption saturation experiment. The results are illustrated in figure 6. The kinetics of the differential absorption is plotted in a semi-log scale. It is clearly linear, the recovery time $\tau = 890 \pm 10$ ns for the GC heat-treated at 700 °C for 24 h. This value is ~2 times longer than that for the Co:$MgAl_2O_4$ single crystal studied for comparison ($\tau = 420$ ns). However, this value is short enough to ensure generation of ns Q-switched pulses for erbium lasers operating at frequencies from few Hz to few kHz.

### 3.5. Q-switching performance

The studied glass-ceramics were tested for Q-switching of an erbium laser. A rod-shaped laser element (diameter: 1.6 mm,

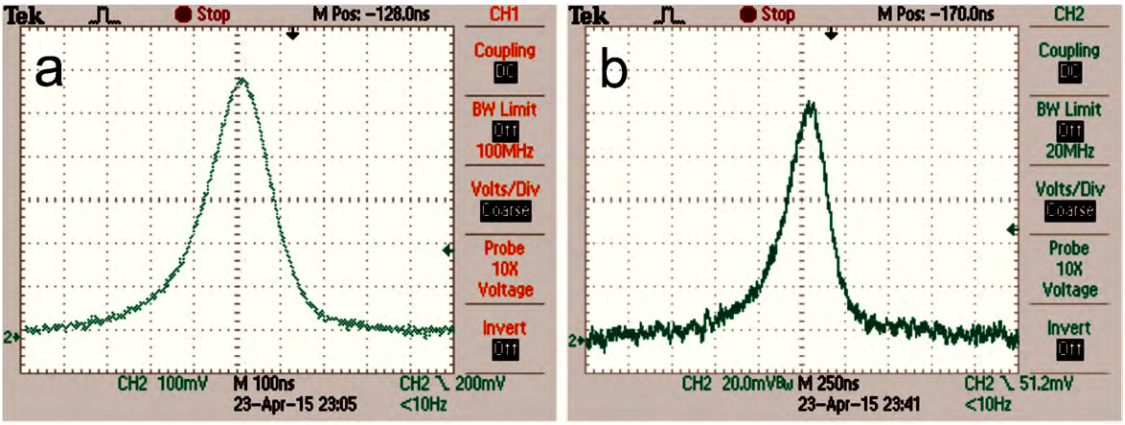


**Figure 7.** Oscilloscope traces of a single Q-switched pulse for the Er,Yb: glass laser when using Co:ZnO based glass-ceramics as a SA: *left* image—GC heat-treated at 680 °C for 18 h, *right* image—GC heat-treated at 700 °C for 4 h.

**Table 1.** Output characteristics[a] of the diode-pumped Er,Yb:glass laser passively Q-switched by the developed glass-ceramics based on Co:ZnO nanocrystals.

| Heat-treatment | $T_0$ (%) | $E_{out}$ (mJ) | $\Delta\tau$ (ns) | $\eta_{conv}$ (%) |
|---|---|---|---|---|
| 680 °C/18 h | 91.5 | 0.37 | 100 | 2.2 |
| 700 °C/4 h | 89.7 | 0.24 | 250 | 0.8 |

[a] $E_{out}$—output pulse energy, $\Delta\tau$—pulse duration, $\eta_{conv}$—Q-switching conversion efficiency.

length: 24 mm) was prepared from a commercial ($Er^{3+}$,$Yb^{3+}$) codoped phosphate glass. Both of its surfaces were anti-reflection (AR) coated for the wavelength ~1.54 $\mu$m. The concentrations of $Er^{3+}$ and $Yb^{3+}$ ions were $0.27 \times 10^{20}$ and $2.5 \times 10^{21}$ atcm$^{-3}$, respectively. The rod was side-pumped by a passively-cooled stack of three 70 W InGaAs laser diode bars emitting at ~940 nm. The duration of the pump pulses was electrically controlled to be ~5 ms, with a pulse repetition frequency of 1 Hz.

The back mirror of the laser cavity was concave (radius of curvature: 1.5 m) and highly reflective (HR) at ~1.54 $\mu$m. The flat output coupler (OC) had a transmission of $T_{OC} = 13\%$. The geometrical cavity length was 65 mm. The SAs were prepared from the glass-ceramics doped with 0.05 wt% CoO and heat-treated at 680 °C and 700 °C, see table 1. Both surfaces of the SAs were AR-coated for the wavelength ~1.54 $\mu$m. The SA was inserted into the laser cavity at normal incidence. The initial transmission of the SAs at 1.54 $\mu$m $T_0$ was 98.7 and 91.5%, respectively. The SA was positioned between the laser rod and the OC. The radius of the laser mode on the SA was ~150 $\mu$m.

The output characteristics of the Er,Yb:glass lasers passively Q-switched with the developed GCs based on the Co:ZnO nanocrystals are shown in table 1. The maximum pulse energy for a single Q-switching pulse $E_{out}$ was 0.37 mJ for the SA made of the GC prepared by the heat-treatment at 680 °C for 18 h. This corresponded to a pulse duration $\Delta\tau$ =100 ns (determined as a full width at half maximum, FWHM). The temporal shape of the Q-switching pulse was close to a Gaussian one (see figure 7). The conversion efficiency with respect to the free-running mode (when the SA was removed from the cavity) was 2.2%; the corresponding pump pulse energy was 0.93 J. The use of the SA obtained by the heat-treatment at 700 °C for 4 h provided much longer pulses ($\Delta\tau = 250$ ns) with a lower pulse energy ($E_{out} = 0.24$ mJ). This is attributed mainly to a lower fraction of Co:ZnO nanocrystals with $Co^{2+}$ ions in tetrahedral sites as compared with the samples prepared at 680 °C for 18 h (see figure 1).

## 4. Conclusions

XRD, Raman and TEM studies and optical spectroscopy of heat-treated glasses of the $K_2O$–ZnO–$Al_2O_3$–$SiO_2$ system doped with CoO revealed crystallization of $Co^{2+}$:ZnO nanocrystals of ~11 nm in size in the residual potassium aluminosilicate glass and entering the $Co^{2+}$ ions into these nanocrystals in the tetrahedral $Zn^{2+}$ positions. The feature of the developed GC is the red-shift of the absorption band related to the $^4A_2(^4F) \rightarrow {}^4T_1(^4F)$ transition of $Co^{2+}$ ions up to ~1.73 $\mu$m. Saturation of absorption is demonstrated within this band (at 1.54 $\mu$m), with a saturation fluence $F_s = 0.8 \pm 0.1$ Jcm$^{-2}$ and recovery time of $890 \pm 10$ ns. The synthesized GC is used to demonstrate passive Q-switching of a diode-pumped Er,Yb:glass laser that generated 0.37 mJ/100 ns pulses at 1.54 $\mu$m. GCs based on $Co^{2+}$:ZnO nanocrystals are promising as a long-wavelength saturable absorber for crystalline erbium lasers emitting at 1.6–1.7 $\mu$m.

## Acknowledgments

O S Dymshits, A A Zhilin, D V Shemchuk and M Ya Tsenter express their gratitude to the RFBR (Grant 16-03-01130) for partial support of this work. This work was also partially supported by the Government of Russian Federation (Grant 074-U01).

## References

[1] Karlsson G, Laurell F, Tellefsen J, Denker B, Galagan B, Osiko V and Sverchkov S 2002 *Appl. Phys.* B **75** 41–6
[2] Tolstik N A, Kurilchik S V, Kisel V E, Kuleshov N V, Maltsev V V, Pilipenko O V, Koporulina E V and Leonyuk N I 2007 *Opt. Lett.* **32** 3233–5

[3] Gorbachenya K N, Kisel V E, Yasukevich A S, Maltsev V V, Leonyuk N I and Kuleshov N V 2013 *Opt. Lett.* **38** 2246–8
[4] Chen Y J, Lin Y F, Huang J H, Gong X H, Luo Z D and Huang Y D 2013 *Laser Phys.* **23** 095801
[5] Loiko P A, Filippov V V, Kuleshov N V, Leonyuk N I, Maltsev V V and Yumashev K V 2014 *Appl. Phys.* B **117** 577–83
[6] Mlynczak J and Belghachem N 2015 *Laser Phys. Lett.* **12** 045803
[7] Karlsson G, Pasiskevicius V, Laurell F, Tellefsen J A, Denker B, Galagan B I, Osiko V V and Sverchkov S 2000 *Appl. Opt.* **39** 6188–92
[8] Kisel V E, Gorbachenya K N, Yasukevich A S, Ivashko A M, Kuleshov N V, Maltsev V V and Leonyuk N I 2012 *Opt. Lett.* **37** 2745–7
[9] Ter-Gabrielyan N, Fromzel V, Lukasiewicz T, Ryba-Romanowski W and Dubinskii M 2011 *Opt. Lett.* **36** 1218–20
[10] Yang X F, Shen D Y, Zhao T, Chen H, Zhou J, Li J, Kou H M and Pan Y B 2011 *Laser Phys.* **21** 1013–6
[11] Kim J W, Shen D Y, Sahu J K and Clarkson W A 2008 *Opt. Express* **16** 5807–12
[12] Volk Yu V, Denisov I A, Malyarevich A M, Yumashev K V, Dymshits O S, Shashkin A V, Zhilin A A, Kang U and Lee K-H 2004 *Appl. Opt.* **43** 682–7
[13] Denisov I A, Volk Yu V, Malyarevich A M, Yumashev K V, Dymshits O S, Zhilin A A, Kang U and Lee K-H 2003 *J. Appl. Phys.* **93** 3827–31
[14] Loiko P A *et al* 2015 *Laser Phys. Lett.* **12** 035803
[15] Pinckney L R 2006 *Phys. Chem. Glass.* **47** 127–30
[16] Alekseeva I P, Dymshits O S, Zhilin A A, Zapalova S S and Shemchuk D V 2006 *J. Opt. Technol.* **81** 723–8
[17] Lipson H and Steeple H 1970 *Interpretation of X-Ray Powder Patterns* (London: Macmillan)
[18] Du X, Zhang H, Cheng C, Zhou S, Zhang F, Yu Y, Dong G and Qiu J 2014 *Opt. Express* **22** 17908–14
[19] Mahmood K, Park S B and Sung H J 2014 *J. Mater. Chem.* C **1** 3138–49
[20] Arguello C A, Rousseau D L and Porto S P S 1969 *Phys. Rev.* **181** 1351–63
[21] Ovsyuk N N and Goryainov S V 2006 *JETP Lett.* **83** 109–12
[22] McMillan P, Piriou B and Navrotsky A 1982 *Geochim. Cosmochim. Acta* **46** 2021–37
[23] Matson D W, Sarma S K and Fhilpotts J A 1986 *Am. Mineral.* **71** 694–704
[24] Kang U, Dymshits O S, Zhilin A A, Chuvaeva T I and Petrovsky G T 1996 *J. Non-Cryst. Solids* **204** 151–7
[25] Alekseeva I, Baranov A, Dymshits O, Ermakov V, Golubkov V, Tsenter M and Zhilin A 2011 *J. Non-Cryst. Solids* **357** 3928–39
[26] Bates T 1962 *Modern Aspects of the Vitreous State* ed J D Mackenzie (London: Butterworths) pp 195–254
[27] Bamford C R 1997 *Colour Generation and Control in Glass* (Amsterdam: Elsevier)
[28] Hunault M, Calas G, Galoisy L, Lelong G and Newville M 2014 *J. Am. Ceram. Soc.* **97** 60–2
[29] Keppler H and Bagdassarov N 1999 *Chem. Geol.* **158** 105–15
[30] Peng Y Z, Liew T, Song W D, An C W, Teo K L and Chong T C 2005 *J. Supercond.* **18** 97–103
[31] Guo S, Zhang X, Huang Y, Li Y and Du Z 2008 *Chem. Phys. Lett.* **459** 82–4